Journal of
Composites Science

MDPI

Article

Numerical Investigation of the Earthquake Response of Rearing Jib Tower Crane Made of Composite Materials with the Adoption of Joint Dampers

Ivan Tomasi [1], Luigi Solazzi [1,*] and Xiangwei Liu [2]

[1] Department of Mechanical and Industrial Engineering, University of Brescia, Via Branze 38, 25123 Brescia, Italy; ivan.tomasi@unibs.it
[2] Logistics Engineering College, Shanghai Maritime University, Haigang Road No. 1550, Shanghai 201306, China; xwliu@shmtu.edu.cn
* Correspondence: luigi.solazzi@unibs.it

Abstract

Tower cranes are highly vulnerable to seismic excitation owing to their slender geometry and pronounced dynamic behaviour. Although carbon fibre reinforced polymer (CFRP) materials offer significant lightweight potential, and damping devices are widely adopted for seismic protection, their combined application to tower cranes has received limited attention. This study numerically investigates the seismic response of a rearing jib tower crane equipped with a CFRP jib and base joint dampers. A finite element model was developed and analysed under four critical operating configurations through static structural, modal and response spectrum analyses in accordance with the Italian Building Code (NTC 2018). The performance of the CFRP solution was compared with that of a conventional steel crane, while two damper configurations with different stiffness values were also assessed. The proposed lightweight design reduced the total crane mass by 34% and the jib weight by 77%. Compared with the steel configuration, the CFRP solution decreased static displacements by 38–56% and equivalent stresses by 22–44%. Under seismic loading, the adoption of joint dampers reduced the maximum equivalent stress by up to 35%, while increasing structural displacements by 5–19% because of the lower support stiffness. The results demonstrate that combining CFRP lightweight design with seismic damping devices effectively improves the earthquake performance of tower cranes while maintaining structural safety.

Keywords: rearing jib tower crane; composite materials; lightweight; finite element analysis; weight reduction; damper;seismic actions

Check for updates

Received: 5 June 2026
Revised: 24 August 2026
Accepted: 1 September 2026
Published: 9 September 2026

Copyright: © 2026 by the authors. Licensee MDPI, Basel, Switzerland. This article is an open access article distributed under the terms and conditions of the Creative Commons Attribution (CC BY) license.

1. Introduction

Cranes represent critical infrastructure in industrial plants, ports, and construction sites, where their structural integrity is essential for both operational continuity and safety. Despite their importance, cranes are often characterised by slender configurations, significant mass eccentricities, and pronounced dynamic sensitivity, making them particularly vulnerable to inertia actions due to the movement of loads [1,2] and environmental actions such as wind loads [3,4] and seismic excitation [5]. Earthquake-induced actions can lead to large displacements, instability phenomena, and damage to both structural and mechanical components [6], highlighting the need for advanced mitigation strategies to avoid a possible collapse of the crane itself [7].

Focusing on this critical issue for the considered structures, several studies have been conducted to analyse the mechanical behaviour of cranes subjected to seismic loads, adopting different methodologies such as the finite element method (FEM) [8–10] or experimental tests on scale models [11–14].

In recent years, increasing attention has been directed towards enhancing the seismic performance of such structures through vibration control technologies [15]; moreover, with an eye kept on weight reduction design, the application of lighter innovative materials to these structures must be considered, while also observing earthquake actions. Fibre-reinforced polymer composites have emerged as a viable solution for structural strengthening and retrofitting due to their high specific strength, low weight, and ease of application. These materials are already implemented in several industrial fields, for example in aircraft structures [16], automotive [17] and also marine applications [18], but in crane design the application of these materials is still under study. Their primary role in crane structures is to reduce overall mass while maintaining or improving structural capacity, thereby limiting inertial forces generated during seismic events, rather than directly contributing to vibration damping [19,20].

Concurrently, to mitigate the seismic effects, seismic isolation devices [21], dynamic vibration absorbers [22,23] or hybrid absorbers [24,25] can be adopted. Seismic protection systems such as base isolation and energy dissipation devices have demonstrated significant effectiveness in reducing the dynamic response of structures [26–28]. In particular, the implementation of base-installed dampers allows for the attenuation of seismic energy before it propagates through the structure, thereby limiting accelerations and internal force demands. When applied to cranes, such systems may provide substantial benefits in terms of stability and serviceability during and after seismic events.

Previous research studies by the authors have already observed the seismic actions on cranes [29,30], the implementation of innovative materials (i.e., CFRP and aluminium) [31,32] and the application of dampers on similar structures [33], but the analysis of these last two features combined has not been properly observed in the scientific literature.

Based on these premises, the main purpose of this research is to carry out a numerical investigation on a rearing jib tower crane made of composite material to understand the earthquake response of the structure, and to show the benefits brought by the application of damping elements also on the structure with innovative materials, compared to the crane made of traditional steel. The main innovation brought by this research paper is the adoption of composite material for these cranes: usually, for the lightweight design of similar structures, the most adopted material is aluminium [34,35] or high-strength steel alloys [36,37]. Here the composite materials, although being more expensive, present higher mechanical properties with lower density. A lighter component means fewer forces and moments for the machine motion (which brings a reduction in energy consumption), easier transportation of the component itself and an increment of safety factors for the other components which have to lift or move these innovative parts. Provided that this damping-system application is effective for this crane category, the proposed methodology can be generalised to other crane variants and subsequently extrapolated to different structural configurations, including composite-material assemblies.

The rest of this research paper has the following structure: Section 2 describes the materials implemented to design the crane and their mechanical properties, focusing also on the numerical model adopted, the configurations studied and the simulations executed. Section 3 shows the results obtained in each simulation conducted, while Section 4 discusses the cited results. At the end, Section 5 summarises the main findings of this research study, also showing the future developments.

2. Materials and Methods

2.1. Materials Implemented

In this research study, a tower crane is analysed in two different configurations: the first one is in steel S355JR, which is a typical structural steel usually adopted for these kinds of applications [38], while the second one has the implementation of carbon fibre reinforced polymer (CFRP). For the junctions between the CFRP tubular elements, aluminium 6061-T6 was adopted because it contributes more effectively to lightweight design than steel. This preliminary selection of the materials was carried out using Ashby's diagrams [39], where the stiffness-density and the strength–density ratios assist in selecting a replacement for the material currently employed in the existing solution, with the aim of reducing the component's weight. As a first approach for the design of the CFRP material, a filament winding process was chosen to evaluate whether the material could withstand the applied loads and could provide a bending stiffness comparable to that of the steel solution (a similar approach was previously proposed in a previous study by the authors [40]). The analysis showed that the constraints were satisfied through the adoption of the carbon fibre M50J [41] and the epoxy resin (a material commonly used with this production process [42]) SX10 [43], resulting in a laminate thickness of 8 mm, which consists of 32 plies (with each ply having a thickness of 0.25 mm). The Layer Stacking Sequence (LSS) includes 20% of the plies oriented at 5°, 20% at −5°, 25% at 45°, 25% at −45°, and 10% at 90°. To provide an overview of the adopted materials, Table 1 summarises the mechanical properties. In particular, the mechanical properties of steel S355JR are in accordance with standard EN 10025 [44], while the mechanical properties of the aluminium 6061-T6 are in accordance with standard EN 755-2 [45]. Regarding the CFRP, it was found that the required mechanical properties are comparable to those of a commercial product, namely a pultruded bar manufactured by Saimex S.r.l., a company based in Milan, Italy, as indicated on their official website. [46]. The corresponding mechanical properties are reported in the cited table. The choice of pultrusion was motivated by its lower manufacturing costs and shorter production times for these components [47,48].

Table 1. Mechanical properties of the materials adopted.

Material	Property	Value	UoM
S355JR	Density	7800	kg/m^3
	Young's Modulus	210,000	MPa
	Poisson's Ratio	0.28	-
	Shear Modulus	7900	MPa
	Yield Strength	355	MPa
CFRP	Density	1900	kg/m^3
	Elastic Modulus [1]	135,000	MPa
	Poisson's Ratio	0.26	-
	Shear Modulus	40,000	MPa
	Tensile strength	2100	MPa
	Ultimate Strain	13	‰
6061-T6	Density	2700	kg/m^3
	Elastic Modulus [1]	69,000	MPa
	Poisson's Ratio	0.33	-
	Shear Modulus	27,000	MPa
	Yield strength	275	MPa

[1] This modulus is evaluated for the longitudinal direction of the pultruded bar.

2.2. Model of the Crane

The lightweight design process was implemented only on the component referred to as the "jib" (see Figure 1 to understand its position), since this component moves during operation. This means that its lightweight redesign leads to a reduction in the dimensions of all the components involved in its movement, thereby reducing energy consumption. Regarding the design phase, already addressed in a previous study by one of the authors [49], since one of the main constraints for this type of component is its deflection [31,50], the redesign of the jib in CFRP must achieve a bending stiffness comparable to that of the steel solution. To achieve this objective, the main design criterion to be fulfilled is expressed by Equation (1):

$$E_{steel} \cdot I_{steel} \approx E_{comp} \cdot I_{comp} \quad (1)$$

For the bending stiffness, E_{steel} is the Young's modulus of the steel, while I_{steel} is the second moment of area of the steel cross-section. Regarding the composite material, E_{comp} is the elastic modulus measured in the longitudinal direction of the pultruded bar, while I_{comp} is the second moment of area of the composite cross-section. The application of this equation allows similar bending and buckling behaviour in both solutions, despite being developed with different materials. Figure 2 shows the designed cross-sections for the steel solution and the CFRP solution of the jib component. The uprights and the diagonals are tubular sections with an external diameter of 80 mm for the steel solution (thickness of 3 mm) and 45 mm for the CFRP solution (thickness of 5 mm).

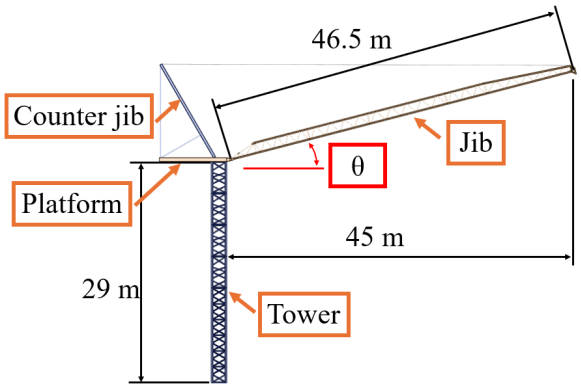
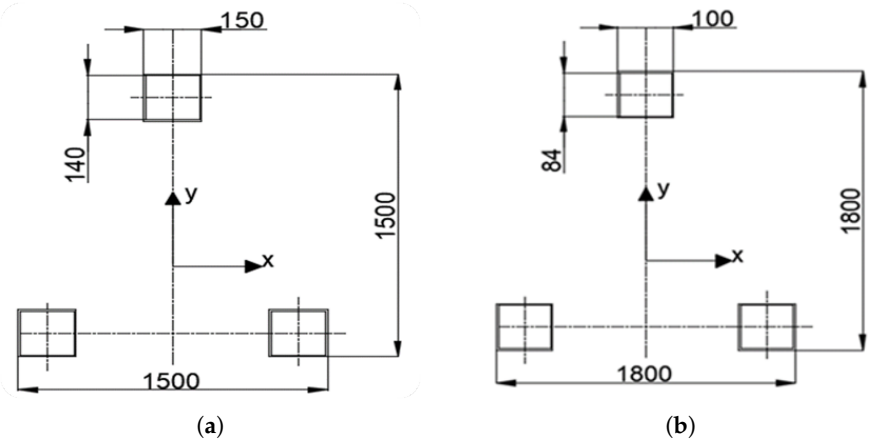


Figure 1. Description of the crane's components.

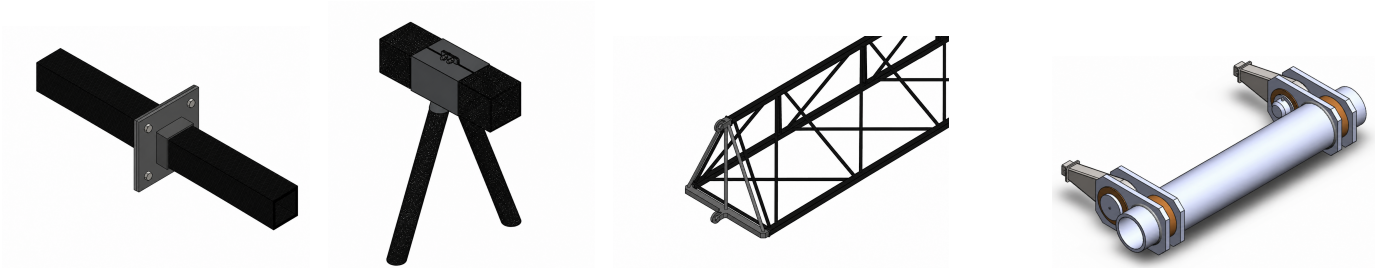


(**a**) (**b**)

Figure 2. Cross sections designed in the two solutions. [mm] (**a**) Steel cross section. (**b**) CFRP cross section.

It should be noted that the square tubular sections of the jib's uprights decrease from 150 mm × 150 mm to 100 mm × 100 mm. With regard to potential wind loads, this reduction in cross-section results in a decrease in wind load on these members by a factor of 1.5, considering that the evaluation of the drag and lift forces induced on a component by the wind is directly proportional to the area exposed to the wind [51,52]. The same reduction factor may reasonably be applied to the entire jib, also considering the diminished dimensions of the diagonal members. This aspect has already been addressed in one of the author's previous papers, which also provides a detailed description of the design phase.

Regarding the joint of the CFRP solution, Figure 3 shows the preliminary design of the junctions adopted to connect the different pultruded bars of the CFRP jib. The joint typology adopted between aluminium and CFRP is an adhesive joint, using a film adhesive as described by Konchakova et al. [53].



(**a**) (**b**) (**c**) (**d**)

Figure 3. Junctions designed in the CFRP solutions. (**a**) Head-to-head junction for tubular elements. (**b**) Diagonal junction with main beam elements. (**c**) End of the jib junction for connection with the pulleys. (**d**) Junction between the jib and the tower.

To understand the whole model adopted, Figure 1 shows the components of the crane. This crane is a cross-linked structure composed mainly of the tower, a jib, a counter-jib and a platform. On this last component, a counterweight is usually placed to move the centre of gravity closer to the tower, avoiding overturning moment effects. The jib can be moved with an angle described by θ between 14.5° and 85°, and the payload was considered equal to 11,000 N, which is the total load, including the payload and all associated accessories. The weight reduction process with composite materials was focused on this specific component. The reason for applying the CFRP material only to the jib is that it is the main component to be moved and which heavily affects the energy consumption for the motion of the machinery.

To understand the weight of the structure, the weight of each component is reported here:

- the tower of the crane: 7869 kg;
- the platform: 4600 kg;
- the counter jib: 4184 kg;
- the counterweight: with a steel jib, a counterweight of 5500 kg is required to ensure stability. However, when the jib is made of composite materials, the required counterweight is drastically reduced—to the point that it can be practically overlooked. This highlights how the lighter weight of the composite jib significantly reduces the balancing demand, leading to major savings in material, transportation, and structural loads;
- the jib: 4937 kg (steel jib) vs. 1134 kg (composite jib).

Regarding the costs of the innovative solution, they were already addressed in a previous study by the author [49]. According to this study, it is well known that manufacturing the jib in composite material entails a significant increase in costs (up to five times that of the steel solution). However, thanks to the weight reduction, the costs associated with the lifting motor, the rotation motor, the ropes, the counterweight, and the lifting operations are reduced, taking

into account electricity costs and a standard load cycle (lifting, rotating, and lowering the jib). Considering these factors, it is noted that the initial cost increase can be offset within the first year, assuming a crane utilisation of 5 h per day and 255 days per year. If the crane is used for 20 years, the estimated economic advantage is more than 500,000 €.

In this research study four configurations of the crane were analysed, with the jib crane in CFRP:

- configuration ANL: the angle θ is equal to 14.5° and the payload is not applied to the structure;
- configuration AL: the angle θ is equal to 14.5° and the payload is applied to the structure;
- configuration BNL: the angle θ is equal to 85° and the payload is not applied to the structure;
- configuration BL: the angle θ is equal to 85° and the payload is applied to the structure.

The reasons behind the choice of these configurations lie between the operational limit of the crane and its most critical conditions: the crane's jib can be lifted with an angle θ between 14.5° and 85°. Furthermore, these angles give the maximum bending moment to the crane (when θ is equal to 14.5°) and the maximum compression (when θ is equal to 85°), which may lead to buckling of the jib. The numerical analyses for the configurations with the jib crane in steel were already addressed in one of the author's previous articles [33]. Moreover, the application at the base of dampers was studied as in the previous article with respect to the condition without the dampers; Table 2 shows their main characteristics. Here, two models of damping elements were analysed to understand the impact of both damping and stiffness values, according to the manufacturer's catalogue [54]. Seismic energy dissipation devices can be categorised into velocity-dependent dampers (e.g., viscous and viscoelastic dampers), displacement-dependent dampers (e.g., hysteretic metallic and friction dampers), and base isolation systems. The dampers considered in this study are from the so-called series "TEC IG", which are elastomeric isolators: they basically consist of a high-damping elastomer core, and laminated steel plates are inserted within the rubber pad as reinforcement. This system is then placed between two steel support plates, which are connected to the ground through four stay rods and to the structure directly linked to the uprights of the crane's tower. In particular, the adopted dampers are simple to install and they are widely implemented in civil engineering structures.

Table 2. Main characteristics of the damping element.

Model	Size [mm]	Vertical Stiffness [kN/mm]	Transversal Stiffness [kN/mm]	Damping Value [Ns/mm]
TEC IG 300 200	350 × 350 × 300	220	0.41	350
TEC IG 400 300	450 × 450 × 400	418	0.49	500

Ansys® 2022 R1 software was used to create a finite element model of the tower crane. Specifically, the model consisted of quadratic beam elements, with roughly 4800 elements and 12,900 nodes. The numbers of elements and nodes described here are the results of a mesh convergence analysis. Considering one of the initial static simulations as an example, it was observed that the increase in the number of elements and nodes adopted led to a variation ofless than 1% in the results compared to the refined solution. The main difference is observed in the computation time: Table 3 shows how the reduction in the number of elements brings significant savings in computational costs.

Table 3. Mesh convergence study of a static structural analysis (configuration AL without dampers).

Element Size [mm]	Elements	Nodes	Time [s]	Total Deformation [mm]
220 (actual solution)	4800	12,900	33	276.63
100	10,000	20,000	54	278.62
50	20,000	58,000	103	278.37
10	100,000	290,000	517	279.01

Regarding the contacts among the elements, bonded contacts were implemented due to the nature of the joints applied. These joints were verified analytically in a previous study by the author [31]. Figure 4 shows the simplified model of the crane in the two positions analysed (ANL/AL and BNL/BL). The difference between AL and ANL is the presence or absence of the payload (the same concept applies to the difference between BL and BNL configurations), always applied to the end of the jib. This payload was defined as a remote mass for all the analyses, and in all the numerical simulations the acceleration of gravity was considered. Regarding the constraints, to understand the influence of the damping elements, fixed supports were first applied (to emulate direct contact with the ground, i.e., without dampers), and then spring elements with stiffness and damping values (reported in Table 2) were adopted to emulate the dampers.

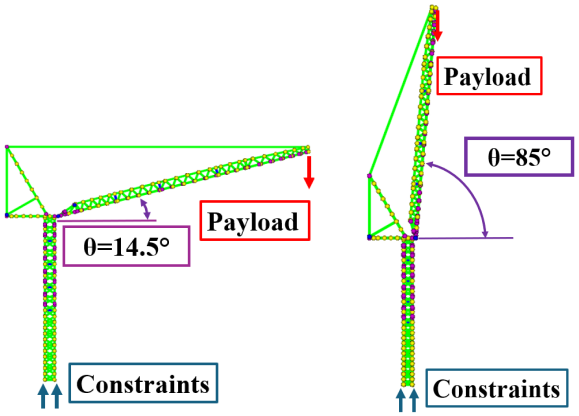


Figure 4. 3D of the simplified model. (**a**) Configuration ANL/AL. (**b**) Configuration BNL/BL.

2.3. Earthquake Actions

Physical dampers are expected to provide benefits for crane structures similar to those observed in buildings, namely a reduction in seismic vibrations (and thus lower accelerations) and an overall improvement in structural performance under earthquake loading.

The seismic response of the crane was assessed according to the Italian Building Code (NTC 2018) [55]. This standard is in line with the Eurocodes [56], a European regulatory framework that offers standardised guidelines for structural design. Ultimate limit states (ULS), which are associated with collapse or instability, and serviceability limit states (SLS), which are related to functionality and durability, are verified in order to evaluate structural safety. The current analysis focuses on the ULS that corresponds to the life safety performance level (SLV), which is determined by a 10% probability of exceedance throughout the reference period. For a nominal service life of 50 years, this corresponds to a return period of approximately 475 years.

The elastic response spectrum, which is dependent on the site-specific seismic hazard, is used to characterise seismic demand. To account for local soil and morphological influences, suitable stratigraphic and topographic amplification factors must be added, because standard spectra apply to idealised reference conditions.

In this study, seismic analyses were performed considering a specific peak ground acceleration (a_g), with a value of $a_g = 0.35g$. In particular, the assumed load spectrum refers to a very high earthquake magnitude in the area of southern Italy, as already described in a previous study by the author [33].

Elastic Design Response Spectrum

The elastic response spectrum, which gives the maximum acceleration of a linear elastic system as a function of its natural period for a certain probability of exceedance, represents the seismic action. The spectrum is defined in normalised form with a reference viscous damping ratio of 5% [57–59], in line with NTC 2018 and the Eurocodes, and is defined by piecewise analytical functions describing the constant-acceleration, constant-velocity, and constant-displacement regions.

The horizontal component is defined in Equations (2)–(5):

$$S_e(T) = a_g\, S\, \eta\, F_0 \left[\frac{T}{T_B} + \frac{1}{\eta F_0}\left(1 - \frac{T}{T_B}\right)\right], \qquad 0 \le T < T_B \tag{2}$$

$$S_e(T) = a_g\, S\, \eta\, F_0, \qquad T_B \le T < T_C \tag{3}$$

$$S_e(T) = a_g\, S\, \eta\, F_0 \left(\frac{T_C}{T}\right), \qquad T_C \le T < T_D \tag{4}$$

$$S_e(T) = a_g\, S\, \eta\, F_0 \left(\frac{T_C\, T_D}{T^2}\right), \qquad T \ge T_D \tag{5}$$

and the vertical component is given by the following Equations (6)–(9):

$$S_{ve}(T) = a_g\, S\, \eta\, F_v \left[\frac{T}{T_B} + \frac{1}{\eta F_v}\left(1 - \frac{T}{T_B}\right)\right], \qquad 0 \le T < T_B \tag{6}$$

$$S_{ve}(T) = a_g\, S\, \eta\, F_v, \qquad T_B \le T < T_C \tag{7}$$

$$S_{ve}(T) = a_g\, S\, \eta\, F_v \left(\frac{T_C}{T}\right), \qquad T_C \le T < T_D \tag{8}$$

$$S_{ve}(T) = a_g\, S\, \eta\, F_v \left(\frac{T_C\, T_D}{T^2}\right), \qquad T \ge T_D \tag{9}$$

where T is the vibration period; a_g is the peak ground acceleration; S is the amplification coefficient accounting for subsoil category and topographic conditions; η is the damping correction factor for viscous damping ratios different from 5%; F_o is the maximum amplification factor of the horizontal spectrum; T_B, T_C, and T_D define the characteristic periods delimiting the different spectral regions; and F_v is the maximum amplification factor of the vertical spectrum. In this study, a Rayleigh damping model characterised by two parameters was assumed. These types of structures show an effective viscous damping magnitude ranging from 0.5% to 5% of the critical damping [59–61]. The value adopted in this study is 5%, which is commonly used in seismic analyses [62,63], and the two coefficients of the Rayleigh model are:

- α = 0.60 s and $\beta = 5.6 \cdot 10^{-4}$ s^{-1} for configurations ANL and AL (configurations at 14.5°);
- α = 0.49 s and $\beta = 6.6 \cdot 10^{-4}$ s^{-1} for configurations BNL and BL (configurations at 85°);

Here α is the stiffness-proportional damping coefficient and β is the mass-proportional damping. Regarding the steel structure, the two coefficients of the Rayleigh model taken

are set to 1.5 and 0.001, respectively, for this structure [64]. Equation (10) describes the evaluation of the damping matrix [C] [65,66]:

$$[C] = \alpha[M] + \beta[K] \tag{10}$$

where [K] is the stiffness matrix of the system and [M] is the mass matrix of the structure.

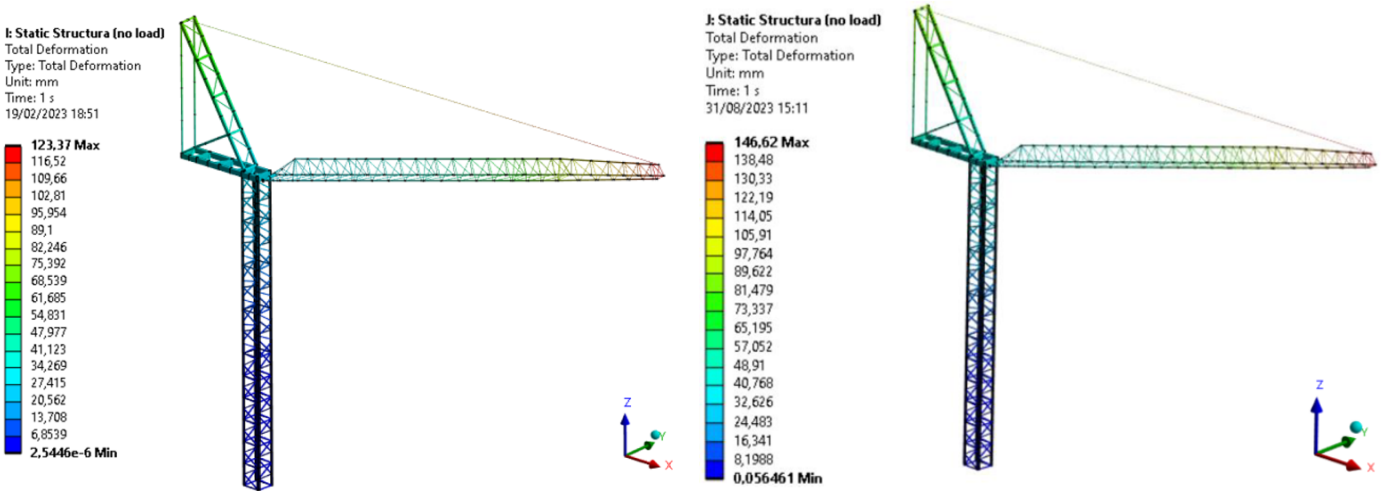
3. Results

3.1. Static Behaviour

In this study, several numerical simulations were run for each configuration considered. In particular, structural static analyses were performed to observe the variation in displacements due to the reduction in stiffness of the entire system, and then modal analyses and response spectrum analyses were conducted to understand the mechanical behaviour of the structure under seismic loading.

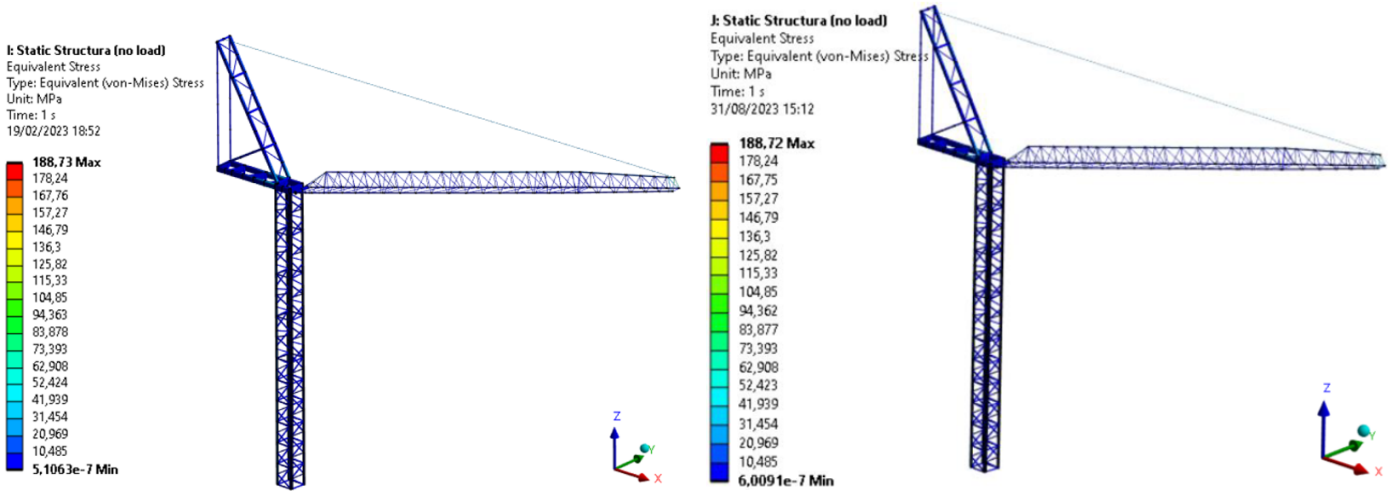
This section reports the static behaviour of the crane, i.e., the crane's mechanical performance under the payload applied at the end of the jib. Figure 5 shows the results of static structural analyses for configuration ANL with and without dampers. It can be observed that the presence of the dampers increases the total displacements of the structure (measured at the end of the jib), while keeping the stress of the crane constant (the maximum value of the stress was also observed at the end of the jib). It should be noted that, for each configuration, total displacements and von Mises stress were shown to better interpret the reported results and to appreciate the improvements brought to the crane by the application of composite materials and dampers.

Figure 6 shows the results of static structural analyses for configuration AL with and without dampers. The difference from the results shown in Figure 5 is that the presence of the applied load increases the total displacements, while the stress evaluation shows almost no change. Also in this case, the presence of the dampers causes a reduction in the stiffness of the entire structure, highlighted by the increase in total displacements (which is of the same order of magnitude as the previous results).



(**a**) (**b**)

Figure 5. *Cont.*

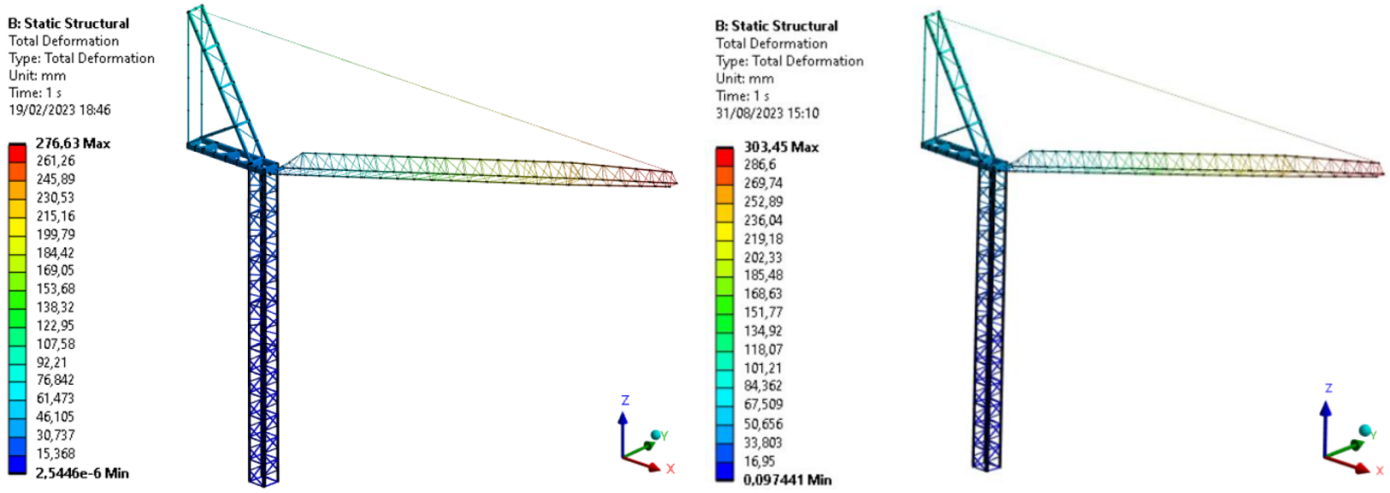


(**c**) (**d**)

Figure 5. Stress and total displacements of static structural simulations for configuration ANL with and without dampers. (**a**) Total displacements of configuration ANL without dampers. (**b**) Total displacements of configuration ANL with dampers. (**c**) Equivalent stress of configuration ANL without dampers. (**d**) Equivalent stress of configuration ANL with dampers.

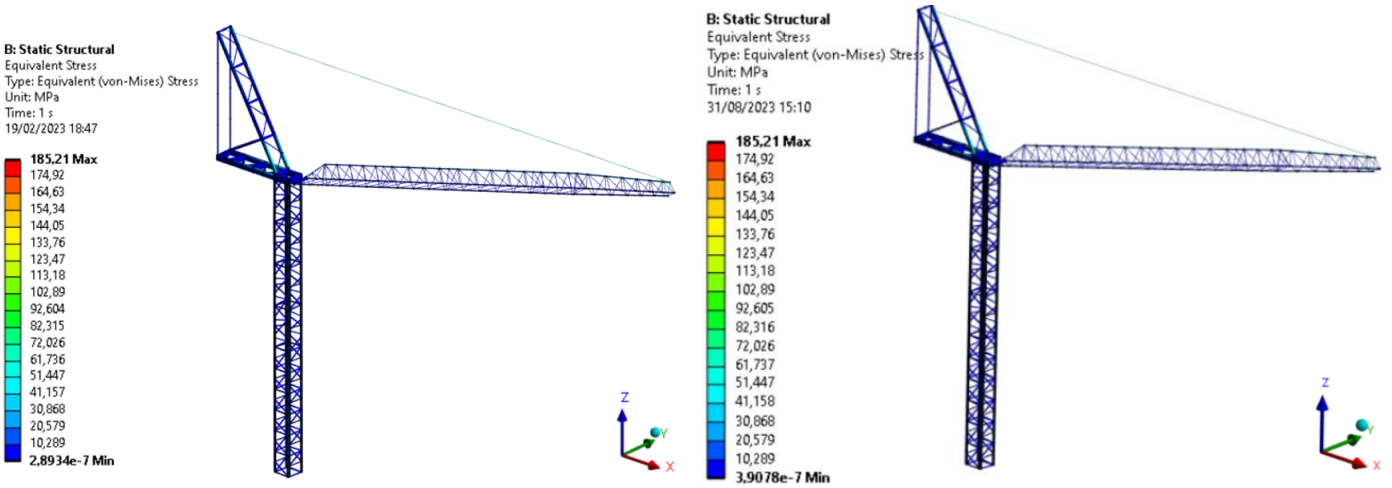
Figure 7 shows the results of static structural analyses for configuration BNL with and without dampers. In this configuration and the next one, the position of the crane differs from the previously illustrated figures. It is possible to see a difference in stress and total displacements evaluated; however, similar results can be observed in this new position: the evaluated stresses were found to be constant with and without the presence of damping elements, while there is an increment of total displacements when the dampers are applied.

Figure 8 shows the results of static structural analyses for configuration BL with and without dampers. Even here the results confirm what happened in the previous three configurations analysed. In these last two configurations (BL and BNL) the position of the maximum stress evaluated is on the counter jib, next to the connection with the platform, while the maximum total displacement evaluated always lies at the end of the jib.



(**a**) (**b**)

Figure 6. *Cont.*

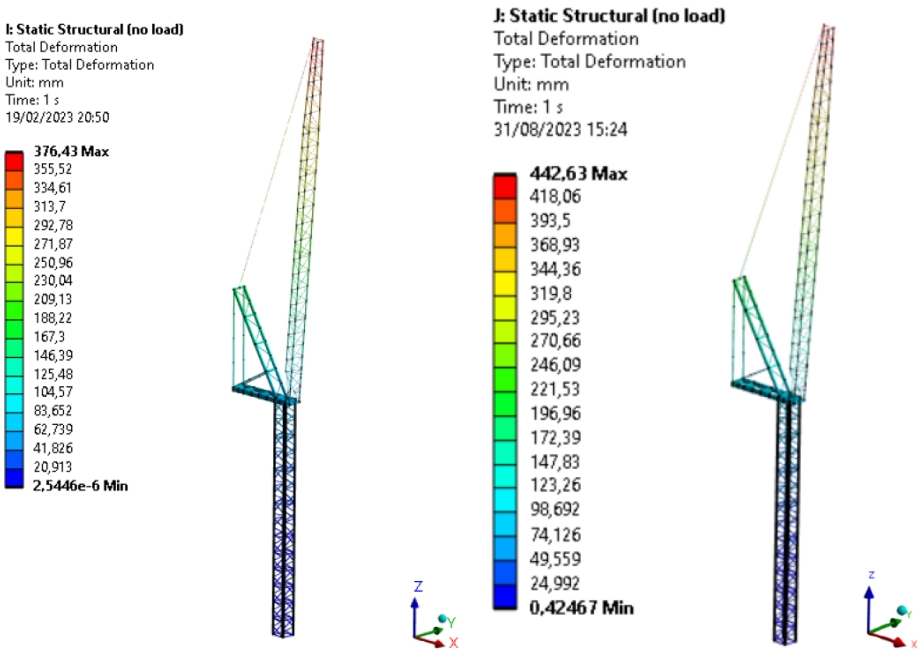


(**c**) (**d**)

Figure 6. Stress and total displacements of static structural simulations for configuration AL with and without dampers. (**a**) Total displacements of configuration AL without dampers. (**b**) Total displacements of configuration AL with dampers. (**c**) Equivalent stress of configuration AL without dampers. (**d**) Equivalent stress of configuration AL with dampers.

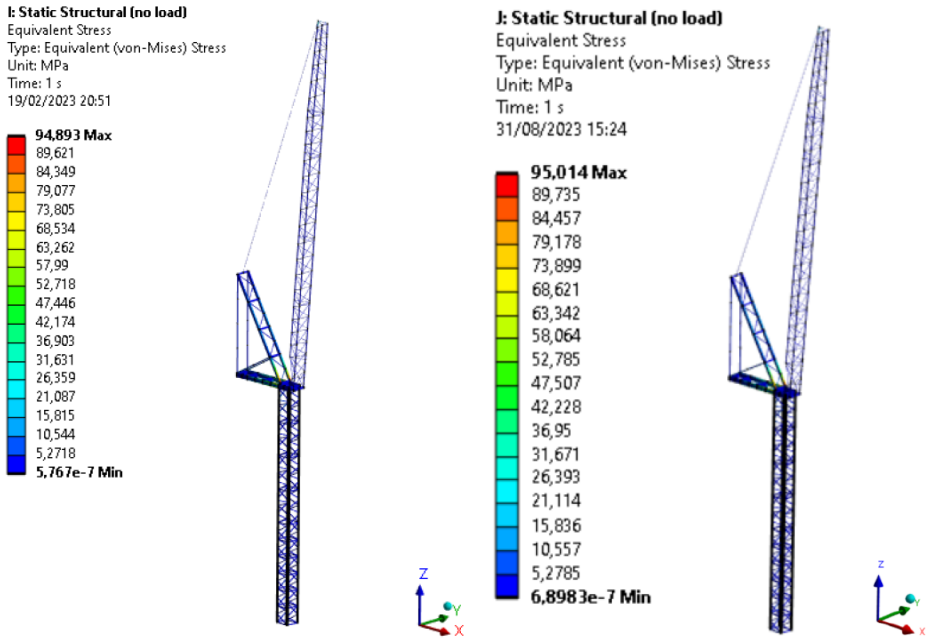
3.2. Modal Analyses

This section reports the main results concerning the modal analyses. Table 4 shows the values of natural frequencies for the first ten modes of the configuration defined as ANL, while Figure 9 shows the first two significant vibration modes of the structure. It should be highlighted that the type of vibration mode is almost the same for the crane with dampers as for the system without damping elements; the only difference observed is in the value of the natural frequency, which is lower for the structure with dampers due to the reduction in stiffness of the entire system. It is worth noting that the values of the first ten natural frequencies are always less than 5–6 Hz, which is in line with the typical values for hoisting machines [64,67].



(**a**) (**b**)

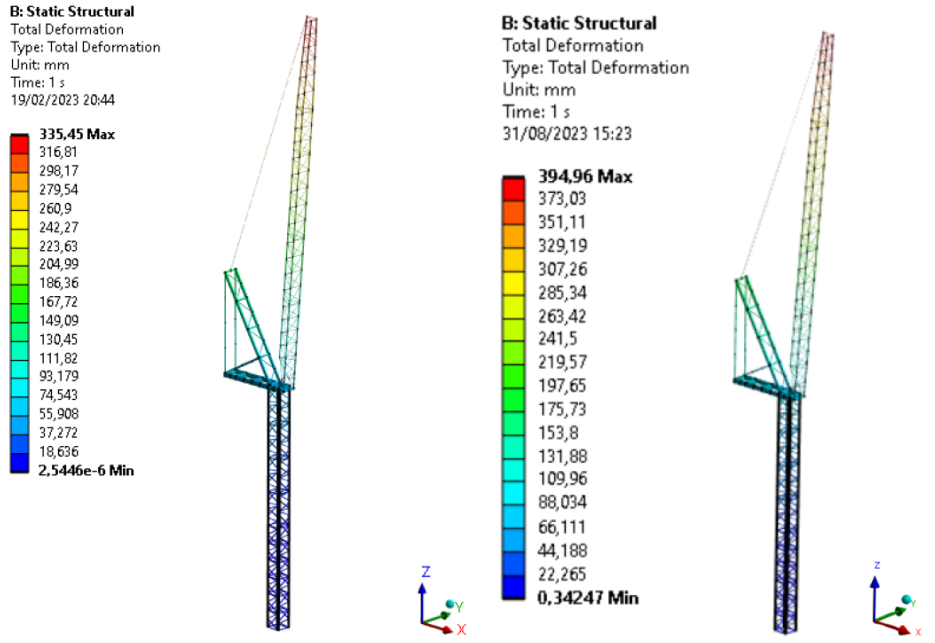
Figure 7. *Cont.*



(**c**) (**d**)

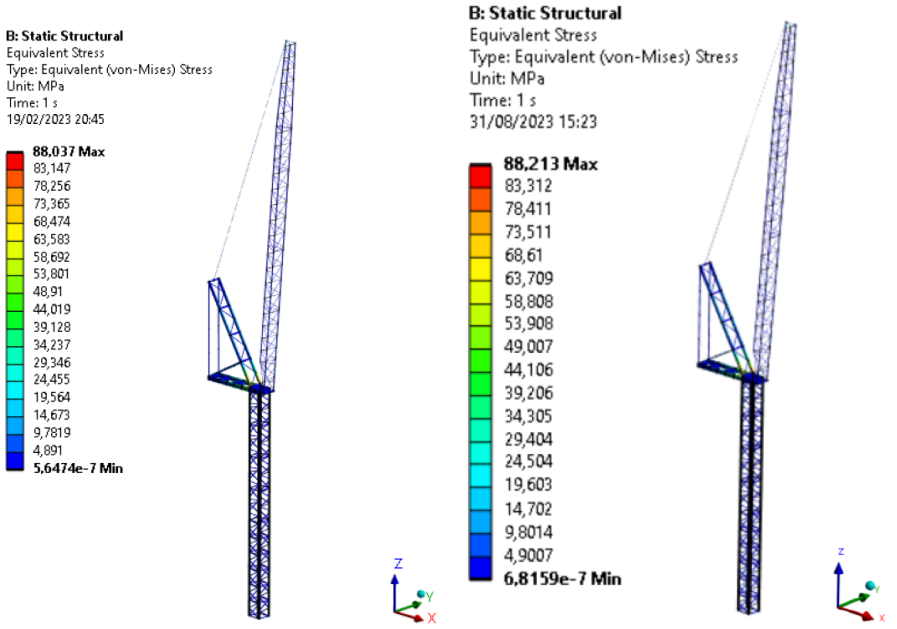
Figure 7. Stress and total displacements of static structural simulations for configuration BNL with and without dampers. (**a**) Total displacements of configuration BNL without dampers. (**b**) Total displacements of configuration BNL with dampers. (**c**) Equivalent stress of configuration BNL without dampers. (**d**) Equivalent stress of configuration BNL with dampers.

Regarding configuration AL, Table 5 shows the values of natural frequencies for the first ten modes, while Figure 10 shows the first two significant modes of vibration of this configuration. Also here the same comments as for the previously analysed configuration can be applied in this scenario, with the difference that the natural frequencies registered had lower values due to the presence of the mass of the payload.



(**a**) (**b**)

Figure 8. *Cont.*



(**c**) (**d**)

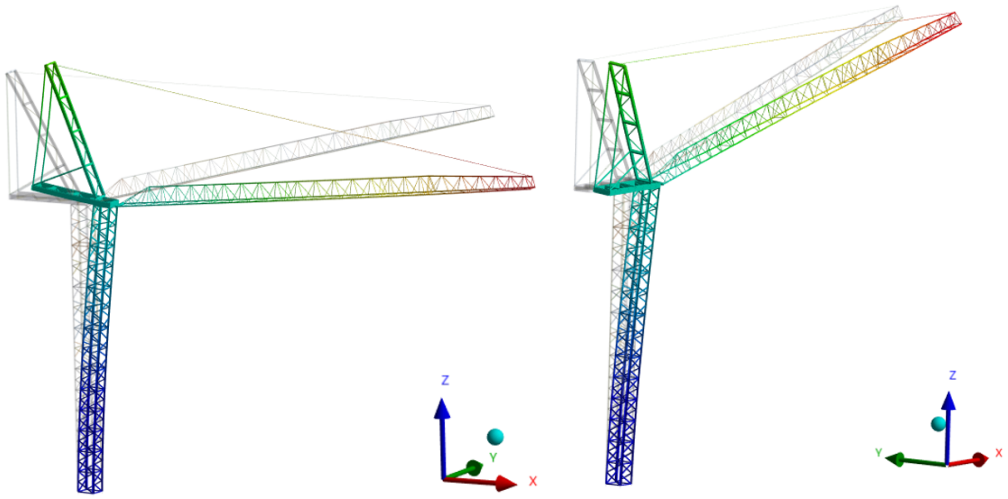
Figure 8. Stress and total displacements of static structural simulations for configuration BL with and without dampers. (**a**) Total displacements of configuration BL without dampers. (**b**) Total displacements of configuration BL with dampers. (**c**) Equivalent stress of configuration BL without dampers. (**d**) Equivalent stress of configuration BL with dampers.

Table 4. First ten significant modes of vibration for ANL configuration.

Mode	Frequency [Hz]	
	No Damping System	Damping System
1	0.596	0.504
2	0.646	0.539
3	1.063	1.063
4	1.659	1.574
5	2.286	2.265
6	2.598	2.596
7	2.865	2.758
8	4.050	4.008
9	4.215	4.129
10	4.840	4.832

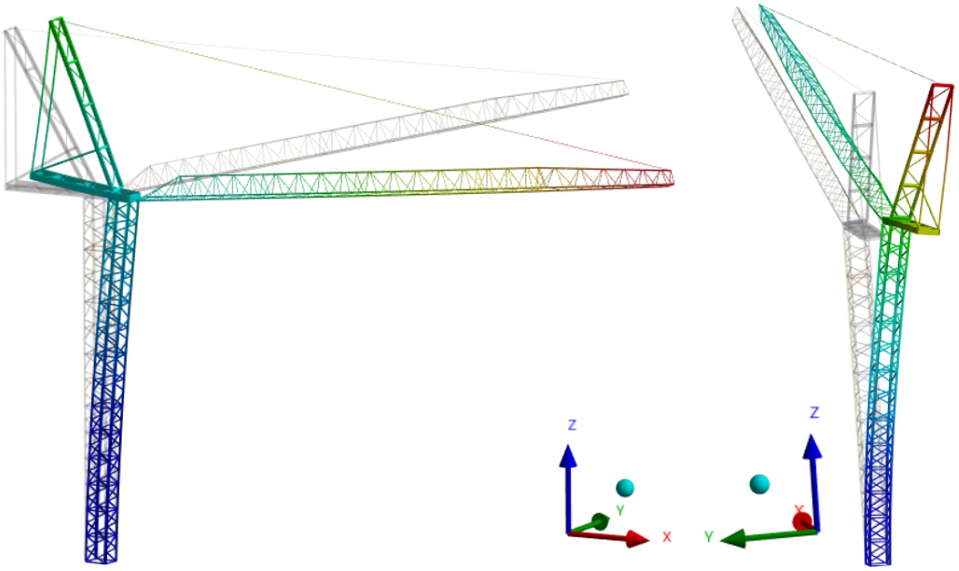
Table 5. First ten modes of vibration for AL configuration.

Mode	Frequency [Hz]	
	No Damping System	Damping System
1	0.481	0.421
2	0.613	0.515
3	1.153	1.149
4	1.276	1.165
5	2.084	2.065
6	2.258	2.256
7	2.884	2.799
8	3.987	3.964
9	4.189	4.077
10	5.508	5.439



(**a**) (**b**)

Figure 9. First two significant vibration's modes for configuration ANL. (**a**) First mode with $f_{n,1}$ = 0.596 Hz (0.504 Hz for configuration with dampers). (**b**) Second mode with $f_{n,2}$ = 0.646 Hz (0.539 Hz for configuration with dampers).



(**a**) (**b**)

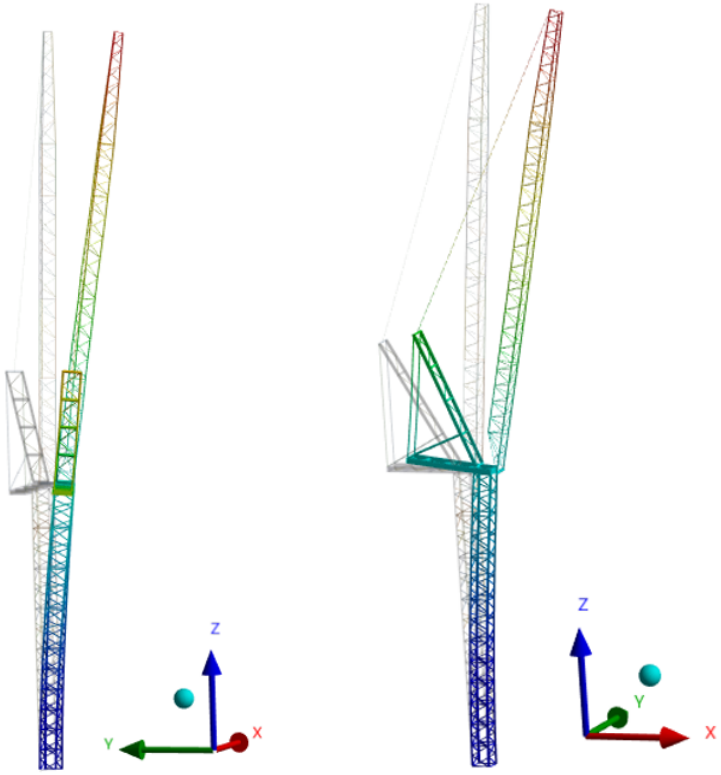
Figure 10. First two significant vibration's modes for configuration AL. (**a**) First mode with $f_{n,1}$ = 0.481 Hz (0.421 Hz for configuration with dampers). (**b**) Second mode with $f_{n,2}$ = 0.613 Hz (0.515 Hz for configuration with dampers).

Considering configuration BNL, Table 6 shows the values of natural frequencies for the first ten modes, while Figure 11 shows the first two significant modes of vibration of this configuration.

Focusing on configuration BL, Table 7 shows the valuevalue of natural of natural frequencies for the first ten modes, while Figure 12 shows the first two significant modes of vibration of this configuration.

Table 6. First ten modes of vibration for BNL configuration.

Mode	Frequency [Hz]	
	No Damping System	Damping System
1	0.478	0.426
2	0.579	0.488
3	0.733	0.724
4	1.444	1.427
5	2.080	1.909
6	2.100	1.966
7	3.033	3.001
8	3.679	6.656
9	4.155	4.153
10	4.261	4.260

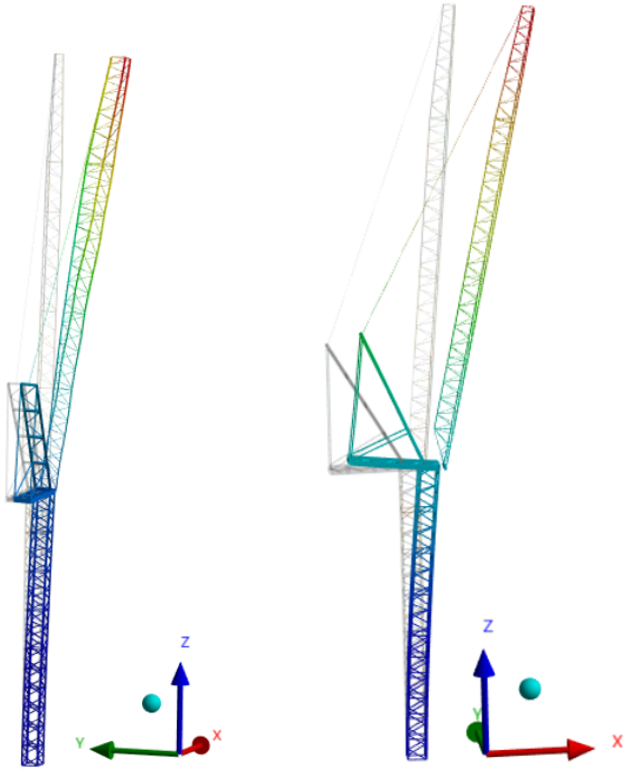


(**a**) (**b**)

Figure 11. First two significant vibration's modes for configuration BNL. (**a**) First mode with $f_{n,1}$ = 0.478 Hz (0.426 Hz for configuration with dampers). (**b**) Second mode with $f_{n,2}$ = 0.579 Hz (0.488 Hz for configuration with dampers).

Table 7. First ten modes of vibration for BL configuration.

Mode	Frequency [Hz]	
	No Damping System	Damping System
1	0.338	0.318
2	0.448	0.390
3	0.504	0.477
4	1.431	1.386
5	1.527	1.402
6	1.857	1.751
7	2.717	2.631
8	3.393	3.346
9	3.912	3.906
10	4.271	4.268



(**a**) (**b**)

Figure 12. First two significant vibration's modes for configuration BL. (**a**) First mode with $f_{n,1}$ = 0.338 Hz (0.318 Hz for configuration with dampers). (**b**) Second mode with $f_{n,2}$ = 0.448 Hz (0.390 Hz for configuration with dampers).

3.3. Seismic Loads

Regarding the earthquake actions, total displacements and stresses were evaluated using response spectrum analyses (RSA). These analyses are used to estimate the peak response of a structure during an earthquake by applying a smoothed spectrum of peak responses from multiple earthquakes to a multi-degree-of-freedom system. By calculating the maximum contributions from each vibration mode separately, the modal maxima are then combined using the complete quadratic combination to obtain a total peak response. For configuration ANL, Figure 13 shows the total displacements and the equivalent stress of the structure, with and without the application of damping elements. From these results, it can be seen that the total displacements increase when the dampers are applied, while there is a reduction in equivalent stress.

Regarding configuration AL, Figure 14 shows the total displacements and the equivalent stress of the structure, with and without the application of damping elements. From these results it can be seen that the total displacements are increased when the dampers are applied, while there is a reduction of equivalent stress, as was observed in the previous configuration. The notable difference is that here, with the application of the payload, the increment of total displacement and reduction of stress is reduced than in the scenario without the payload.

Considering configuration BNL, Figure 15 shows the total displacements and the equivalent stress of the structure, with and without the application of the damping element. From these results it can be seen that the total displacements are increased when the dampers are applied, while there is a reduction of equivalent stress.

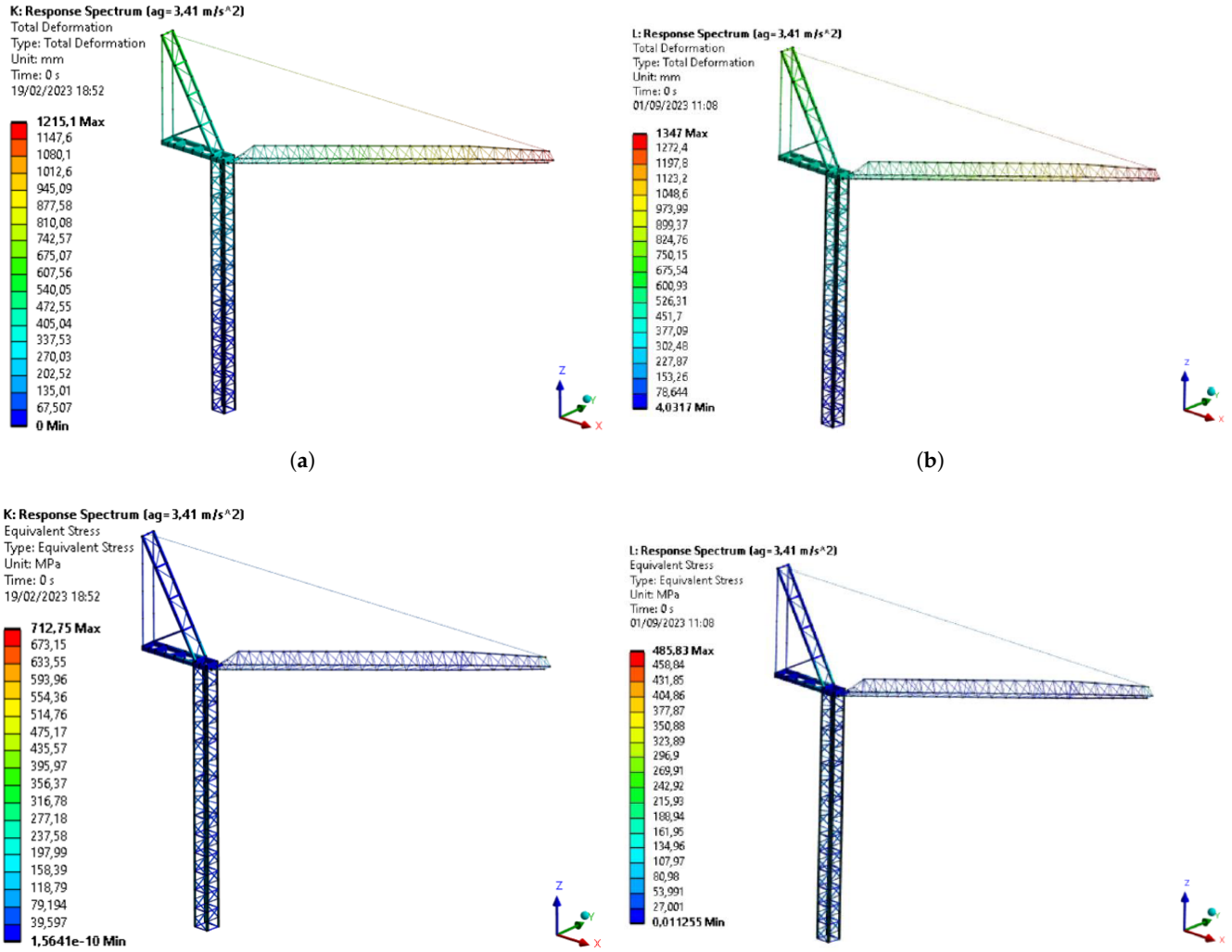


Figure 13. Stress and total displacements of RSA simulations for configuration ANL with and without dampers. (**a**) Total displacements of configuration ANL without dampers. (**b**) Total displacements of configuration ANL with dampers. (**c**) Equivalent stress of configuration ANL without dampers. (**d**) Equivalent stress of configuration ANL with dampers.

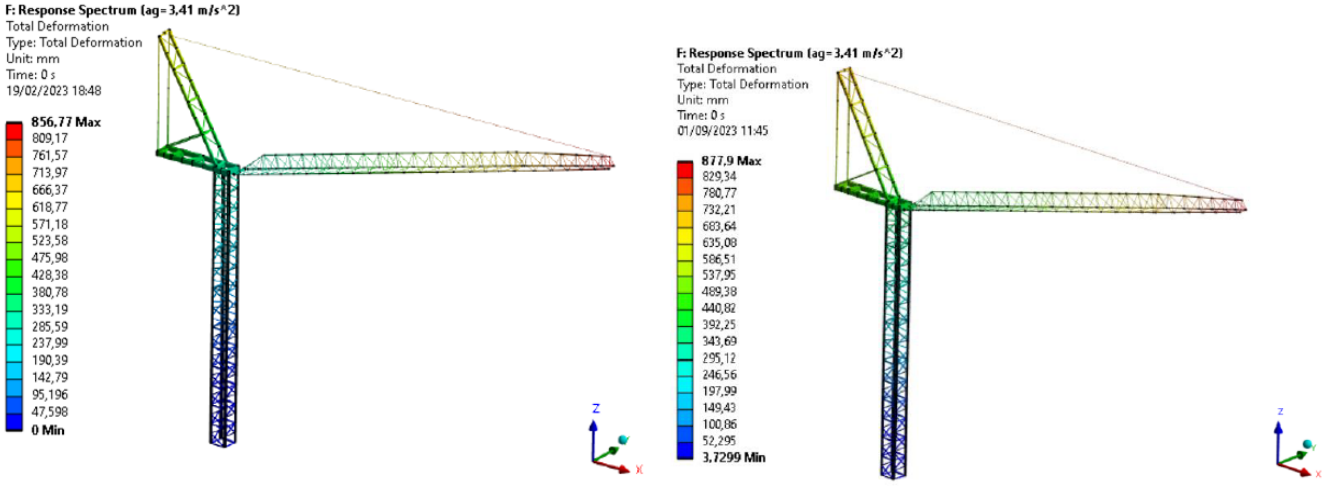
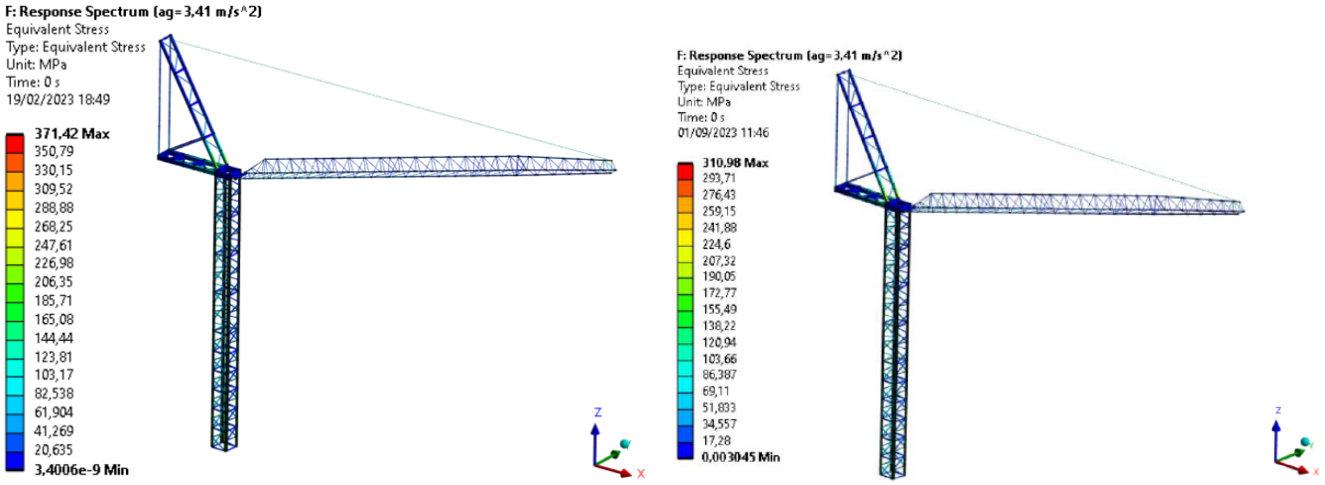
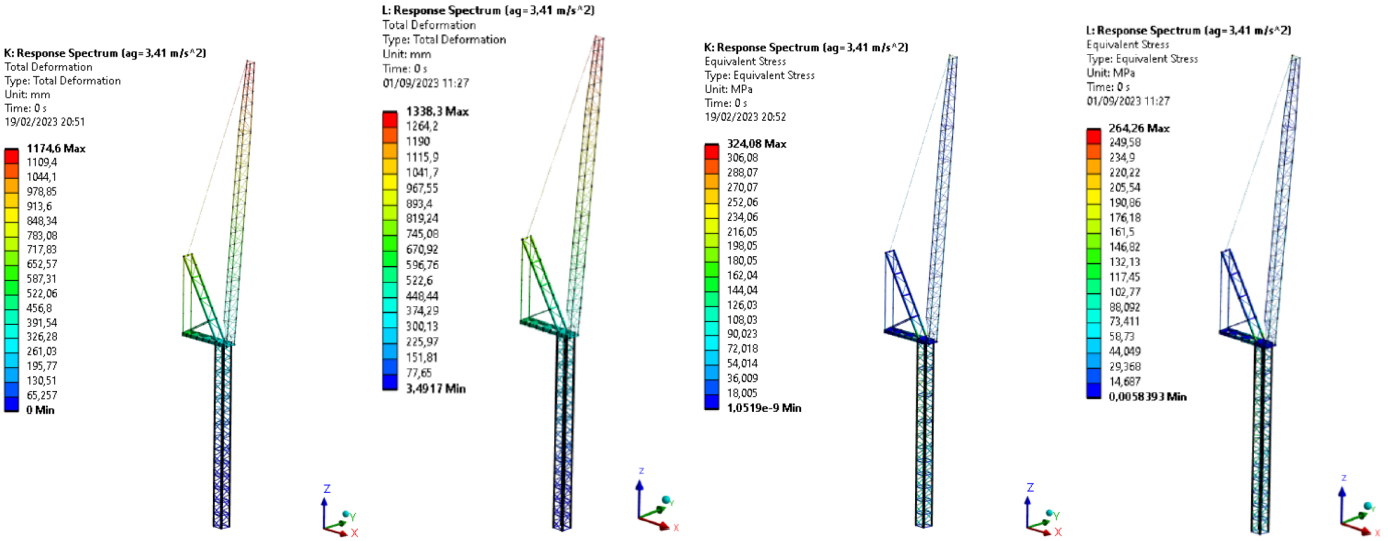


Figure 14. *Cont.*



(**c**) (**d**)

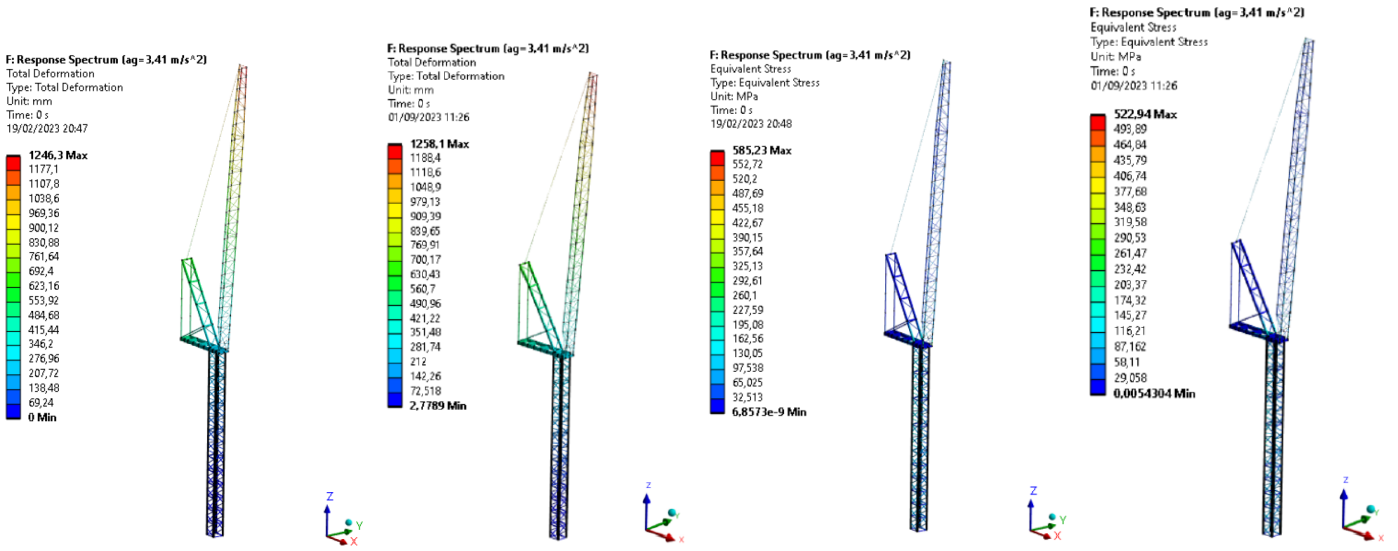
Figure 14. Stress and total displacements of RSA simulations for configuration AL with and without dampers. (**a**) Total displacements of configuration AL without dampers. (**b**) Total displacements of configuration AL with dampers. (**c**) Equivalent stress of configuration AL without dampers. (**d**) Equivalent stress of configuration AL with dampers.



(**a**) (**b**) (**c**) (**d**)

Figure 15. Stress and total displacements of RSA simulations for configuration BNL with and without dampers. (**a**) Total displacements of configuration BNL without dampers. (**b**) Total displacements of configuration BNL with dampers. (**c**) Equivalent stress of configuration BNL without dampers. (**d**) Equivalent stress of configuration BNL with dampers.

Focusing on configuration BL, Figure 16 shows the total displacements and the equivalent stress of the structure, with and without the application of the damping element. From these results it can be seen that the total displacements are increased when the dampers are applied, while there is a reduction of equivalent stress.



(**a**) (**b**) (**c**) (**d**)

Figure 16. Stress and total displacements of RSA simulations for configuration BL with and without dampers. (**a**) Total displacements of configuration BL without dampers. (**b**) Total displacements of configuration BL with dampers. (**c**) Equivalent stress of configuration BL without dampers. (**d**) Equivalent stress of configuration BL with dampers.

4. Discussion

This section summarises the results obtained, and then different comparisons are highlighted. In particular:

- a comparison between the traditional steel crane and the application of composite material;
- a comparison between the structure in composite material with and without the application of damping elements;
- a comparison between two different types of dampers.

The first comparison can be done on the weight of the structure: considering a total weight of the steel crane of 27,090 kg and 17,787 kg for the composite crane, through Equation (11), it is possible to evaluate the reduction $Red_{weight}\%$ of the crane:

$$Red_{weight}\% = \frac{m_{S355JR} - m_{CFRP}}{m_{S355JR}} \cdot 100 \ [\%] \tag{11}$$

where m_{S355JR} is the total mass of the crane made of steel, while m_{CFRP} is the total mass of the crane made of CFRP. The reduction in weight found is 34% for the crane. If we focus only on the weight reduction of the jib, it can be observed a value equal to 77% can be observed. Based also on results already reported in a previous author's research [33], Table 8 shows the results for the static structural analyses for all the configurations studied, observing both the traditional adoption of steel S355JR and CFRP.

Starting with a comparison between the adoption of the composite material with respect to the steel configuration, it is clear that there is a reduction in both total displacements and evaluated stress in each configuration analysed. This reduction $Red_{displ/stress,mat}\%$ can be evaluated through Equation (12):

$$Red_{displ/stress,mat}\% = \frac{\delta/\sigma_{max,S355JR} - \delta/\sigma_{max,CFRP}}{\delta/\sigma_{max,S355JR}} \cdot 100 \ [\%] \tag{12}$$

where $\delta/\sigma_{max,S355JR}$ is the maximum total displacement (or stress) evaluated for the crane model in steel S355JR and $\delta/\sigma_{max,CFRP}$ is the maximum total displacement (or stress)

evaluated for the crane model with the jib in carbon fibre reinforced polymer. It can be evaluated that the composite material implies a reduction in displacement between 38% and 56% compared to the S355JR configurations. Regarding the stress evaluated, a reduction between 22% and 44% is evaluated.

Table 8. Comparison between the results of static structural analyses for the configurations of the crane made of S355JR and CFRP. To understand the acronyms in the column for the adoption of dampers, ND means "no dampers", D1 is the first type of dampers previously shown (TEC IG 300 200) and D2 is the second type of dampers previously shown (TEC IG 400 300).

Static Structural		S355JR [1]		CFRP	
Configuration	**Adoption of Dampers**	**Total Displacement [2] [mm]**	**Equivalent Stress [2] [MPa]**	**Total Displacement [2] [mm]**	**Equivalent Stress [2] [MPa]**
ANL	ND	257.58	243.95	123.37	188.73
	D1	280.11	243.97	146.62	188.72
	D2	269.13	243.96	135.54	188.72
AL	ND	625.55	252.64	276.63	185.21
	D1	703.50	252.71	303.45	185.21
	D2	666.22	252.67	290.66	185.21
BNL	ND	621.57	165.54	376.43	94.89
	D1	730.58	165.94	442.63	95.01
	D2	678.61	165.75	411.16	94.96
BL	ND	582.51	158.95	335.45	88.34
	D1	685.16	159.45	394.96	88.21
	D2	636.19	159.22	366.64	88.13

[1] The values for the steel analyses are already reported in a previous author's research. [2] The values here taken are the maximum values of the structure.

With the aim of a better comprehension of the consequences brought by the adoption of damping elements, the variation of stress and displacement must be observed. To evaluate the reduction $Red_{stress}\%$ of the equivalent Von Mises stress, Equation (13) is shown:

$$Red_{stress}\% = \frac{\sigma_{max,fixed} - \sigma_{max,el}}{\sigma_{max,fixed}} \cdot 100 \ [\%] \tag{13}$$

where $\sigma_{max,fixed}$ is the maximum Von Mises stress evaluated for the fixed supports model and $\sigma_{max,el}$ is the maximum Von Mises stress evaluated for the elastic-damped supports model. A similar method is adopted to compute the reduction $Red_{displ}\%$ of the total displacement, which is described by Equation (14):

$$Red_{displ}\% = \frac{\delta_{max,fixed} - \delta_{max,el}}{\delta_{max,fixed}} \cdot 100 \ [\%] \tag{14}$$

where $\delta_{max,fixed}$ is the maximum total displacement evaluated for the fixed supports model and $\delta_{max,el}$ is the maximum total displacement evaluated for the elastic-damped supports model. Both in steel and in CFRP models, the application of dampers implies an increment of maximum total displacements, between 5% and 19%, while the stresses have negligible variations. In particular the increment is lower when the second type of damping element is applied, probably due to its higher stiffness.

Regarding the modal analyses, the natural frequencies obtained with the CFRP structure are higher than those of the steel model, due to the reduction of weight. With the application of dampers, a reduction of the natural frequencies is observed, in particular with the seismic damper TEC IG 300 200, having with a lower stiffness than the other two systems.

About the response spectrum analyses, Table 9 shows the results for all the configurations studied, observing both the materials adopted for this type of crane.

Table 9. Comparison between the results of RSA for the configurations of the crane made of S355JR and CFRP. To understand the acronyms in the column of the adoption of dampers, ND means "no dampers", D1 is the first type of dampers previously shown (TEC IG 300 200) and D2 is the second type of dampers previously shown (TEC IG 400 300).

Response Spectrum		S355JR [1]		CFRP	
Configuration	Adoption of Dampers	Total Displacement [2] [mm]	Equivalent Stress [2] [MPa]	Total Displacement [2] [mm]	Equivalent Stress [2] [MPa]
ANL	ND	970.94	359.22	1215.10	712.75
	D1	961.88	263.58	1347.00	485.83
	D2	964.64	274.02	1268.20	510.97
AL	ND	886.49	320.34	856.77	371.42
	D1	917.43	297.56	877.90	310.98
	D2	902.46	304.61	866.54	319.88
BNL	ND	1376.80	261.08	1174.60	324.08
	D1	1305.50	218.91	1338.30	264.26
	D2	1295.40	228.34	1284.00	271.95
BL	ND	1314.10	275.31	1246.30	585.23
	D1	1239.30	237.86	1258.10	522.94
	D2	1222.10	245.96	1223.80	540.28

[1] The values for the steel analyses are already reported in a previous author's research. [2] The values here taken are the maximum values of the structure.

Considering the same evaluation for each reduction described by Equation (12) to assess the effect of CFRP application, the displacements were found to vary depending on the configuration analysed, with an increase of up to 40% for configuration ANL with damper D1, while in configuration AL a reduction of less than 5% was observed in all scenarios with and without damping elements. With regard to configurations BNL and BL, there is a reduction in displacements for both configurations with fixed supports, while in the case of dampers, the differences are less than 3%. As for the stress, there is generally an increase in equivalent stress for each configuration studied, but considering the high strength limit of the material, the crane is always in a safe condition. With regard to the variation brought by damping elements in the crane with the composite jib, a slight increase in total displacements is noted, especially when damper D1 is implemented, but a reduction in stress of up to 35% (in configuration ANL) is observed when these devices are applied.

5. Conclusions

The present study presents a numerical investigation on a rearing jib tower crane made of CFRP with joint dampers to better understand seismic actions. The definition of the materials involved, the 3D model, and the configurations analysed, chosen for their critical conditions, provided the framework for a series of numerical simulations which evaluated the static behaviour, the modes of vibration and the response to earthquake accelerations of the studied crane. In particular, a comparison between the two materials analysed on the crane, a comparison between configurations with and without dampers, and a comparison of different dampers (the second being stiffer than the first one) were examined in this study, leading to the following results:

- the implementation of composite material for the jib of the crane allows a weight reduction up to 34%, compared to the structure made all in steel;

- the application of joint dampers at the base brings higher displacements (which can be accepted considering the size of the crane and the needed precision for its purpose) but lower stress, with a peak stress reduction of 35%;
- when damper stiffness is increased, the resulting increase in displacements is smaller; however, the reduction in evaluated stress is also lower (for example, the first type of damper achieves a 35% reduction in stress, while the second type results in approximately a 28% reduction).

The implementation of composite materials significantly contributes to lightweight design when the geometry of the structure is fully optimised. Understanding these environmental actions is crucial for hoisting machines, even more so when the materials applied are not well suited for this field. Furthermore, adopting damping elements can improve the design of these structures, and this improvement is independent of the material used, as demonstrated in this study.

Regarding future developments, the same procedure will be applied to other crane typologies, and different types of dampers can be implemented on the crane, for instance, to reduce the jib's overall deflection. Moreover, other environmental loads can be analysed for a better understanding of the structural behaviour, as already done in previous studies by the authors [68,69]. Furthermore, experimental validation through a scale model is planned, with the design of a specific shake table, as already observed in previous research papers [12–14].

Author Contributions: Conceptualisation, L.S. and X.L.; methodology, L.S.; software, I.T.; validation, L.S. and I.T.; formal analysis, I.T.; investigation, I.T.; resources, L.S.; data curation, I.T.; writing—original draft preparation, I.T.; writing—review and editing, L.S. and I.T.; visualisation, I.T.; supervision, L.S. and X.L.; project administration, L.S.; funding acquisition, L.S. All authors have read and agreed to the published version of the manuscript.

Funding: This research received no external funding.

Informed Consent Statement: Not applicable.

Data Availability Statement: The original contributions presented in the study are included in the article; further inquiries can be directed to the corresponding author.

Conflicts of Interest: The authors declare no conflicts of interest.

Abbreviations

The following abbreviations are used in this manuscript:

CFRP	Carbon Fibre Reinforced Polymer
LSS	Layer Stacking Sequence
ULS	Ultimate Limit States
RSA	Response Spectrum Analysis

References

1. Yang, C.; Huang, J.; Singhose, W. Dynamic modeling and oscillation control of industrial cranes transporting upright slender flexible payloads. *Mech. Syst. Signal Process.* **2024**, *220*, 111676. [CrossRef]
2. Rauscher, F.; Sawodny, O. Modeling and control of tower cranes with elastic structure. *IEEE Trans. Control Syst. Technol.* **2020**, *29*, 64–79. [CrossRef]
3. Chen, W.; Qin, X.; Yang, Z.; Zhan, P. Wind-induced tower crane vibration and safety evaluation. *J. Low Freq. Noise Vib. Act. Control* **2020**, *39*, 297–312. [CrossRef]
4. Urbaś, A.; Stadnicki, J. Dynamics of a knuckle crane carrying a load subjected to wind pressure. *Multibody Syst. Dyn.* **2025**, *65*, 89–118. [CrossRef]

5. Peng, Q.; Cheng, W.M.; Guo, P.; Jia, H. Assessing Seismic Performance of Gantry Crane Subjected to Near-Field Ground Motions Using Incremental Dynamic and Endurance Time Analysis Methods. *Shock Vib.* **2022**, *2022*, 6624530. [CrossRef]
6. Santiago-Fandiño, V.; Sato, S.; Maki, N.; Iuchi, K. *The 2011 Japan Earthquake and Tsunami: Reconstruction and Restoration. Insights and Assessment After 5 Years*; Springer International Publishing: Cham, Switzerland, 2018.
7. Tran, Q.H.; Huh, J.; Doan, N.S.; Mac, V.H.; Ahn, J.H. Fragility assessment of a container crane under seismic excitation considering uplift and derailment behavior. *Appl. Sci.* **2019**, *9*, 4660. [CrossRef]
8. Hu, Z.; Su, Z. Computer-Aided Seismic Analysis of Nuclear Power Plant Overhead Crane. In Proceedings of the 2025 5th International Conference on Computational Modeling, Simulation and Data Analysis, Qingdao, China, 14–16 December 2025.
9. Kenan, H.; Azeloglu, C.O. Seismic performance analysis of tower crane mast types with different bracing configurations. In *Structures*; Elsevier: Amsterdam, The Netherlands, 2021; Volume 34.
10. Meisuh, B.K.; Haldar, A.; Huh, J.; Kim, I.T.; Nguyen, V.B. Nonlinear time domain seismic response and performance evaluation of A-frame jumbo-size container cranes. *Appl. Ocean Res.* **2024**, *142*, 103858. [CrossRef]
11. Nguyen, V.B.; Huh, J.; Meisuh, B.K.; Kim, J.; Park, I.J. Seismic response of container crane under near-field and far-field ground motions. *Appl. Sci.* **2021**, *11*, 1740. [CrossRef]
12. Li, Z.; Ye, F.; Wu, S. Design and experimental verification of a 1/20 scale model of quayside container crane using distortion theory. *Shock Vib.* **2019**, *2019*, 5893948. [CrossRef]
13. Azeloglu, C.O.; Sagirli, A.; Edincliler, A. Mathematical modelling of the container cranes under seismic loading and proving by shake table. *Nonlinear Dyn.* **2013**, *73*, 143–154. [CrossRef]
14. Wang, Z.; Li, S.; Lu, S.; Yu, S. Model investigations for seismic responses of a scaled polar crane at a nuclear power station. *Nucl. Eng. Des.* **2021**, *381*, 111330. [CrossRef]
15. Jaafar, H.I.; Mohamed, Z.; Shamsudin, M.A.; Subha, N.M.; Ramli, L.; Abdullahi, A.M. Model reference command shaping for vibration control of multimode flexible systems with application to a double-pendulum overhead crane. *Mech. Syst. Signal Process.* **2019**, *115*, 677–695. [CrossRef]
16. Rana, S.; Fangueiro, R. (Eds.) *Advanced Composite Materials for Aerospace Engineering: Processing, Properties and Applications*; Woodhead Publishing: Cambridge, MA, USA, 2016.
17. Ravishankar, B.; Nayak, S.K.; Kader, M.A. Hybrid composites for automotive applications—A review. *J. Reinf. Plast. Compos.* **2019**, *38*, 835–845. [CrossRef]
18. Neşer, G. Polymer based composites in marine use: History and future trends. *Procedia Eng.* **2017**, *194*, 19–24. [CrossRef]
19. Suvorov, V.; Vasilyev, R.; Melnikov, B.; Kuznetsov, I.; Bahrami, M.R. Weight reduction of a ship crane truss structure made of composites. *Appl. Sci.* **2023**, *13*, 8916. [CrossRef]
20. Tulekov, A.; Togizbayeva, B.; Kenesbek, I.; Kenesbek, A.; Zabiyeva, A. The Use of Composite Materials in the Production of Tower Cranes. *Acta Polytech. Hung.* **2023**, *20*, 225–240. [CrossRef]
21. Zheng, P. Container Crane Seismic Isolation Device Design Method Based on Structural Dynamics. *Appl. Mech. Mater.* **2013**, *353*, 1819–1825. [CrossRef]
22. Salvi, J.; Rizzi, E.; Rustighi, E.; Ferguson, N.S.. Optimum tuning of passive tuned mass dampers for the mitigation of pulse-like responses. *J. Vib. Acoust.* **2018**, *140*, 061014. [CrossRef]
23. Akbar, M.A.; Wong, W.; Rustighi, E. Design optimization of a single-mass impact damper. *J. Sound Vib.* **2024**, *570*, 118019. [CrossRef]
24. Akbar, M.A.; Wong, W.O.; Rustighi, E. A hybrid damper with tunable particle impact damping and coulomb friction. *Machines* **2023**, *11*, 545. [CrossRef]
25. Salvi, J.; Rizzi, E.; Rustighi, E.; Ferguson, N.S. On the optimization of a hybrid tuned mass damper for impulse loading. *Smart Mater. Struct.* **2015**, *24*, 085010. [CrossRef]
26. Meisuh, B.K.; Huh, J.; Haldar, A.; Kim, I.T. Comparison of seismic responses of a jumbo-size container crane retrofitted with braces, dampers, and isolation systems. *Ocean Eng.* **2022**, *262*, 112222. [CrossRef]
27. Ye, F.; Xue, X.; Jiang, W.; Yin, X. Mechanism and Experimental Investigation of Vibration Reduction for Container Cranes Based on Particle Damping Technology. *Actuators* **2023**, *13*, 11. [CrossRef]
28. Wang, G.; Wang, Y.Y.; Yuan, J.; Yang, Y.; Wang, D. Arc-Surfaced Frictional Damper for Vibration Control in Container Crane. *Shock Vib.* **2017**, *2017*, 3675470. [CrossRef]
29. Solazzi, L. Ship to shore crane subjected to earthquake. *Procedia Eng.* **2011**, *10*, 2690–2695. [CrossRef]
30. Solazzi, L.; Danzi, N. Dynamic effects on the lattice boom crane due to the wind, moving load and earthquake events. *U.Porto J. Eng.* **2023**, *9*, 109–124. [CrossRef]
31. Solazzi, L.; Tomasi, I. Design of an overhead crane in steel, aluminium and composite material using the prestress method. *J. Compos. Sci.* **2024**, *8*, 380. [CrossRef]
32. Solazzi, L. Feasibility study of a very big crawler crane using composite materials. *Compos. Part C Open Access* **2024**, *13*, 100430. [CrossRef]

33. Solazzi, L.; Rustighi, E. Passive Earthquake Vibration Mitigation of a Steel Tower Crane by Joint Dampers. *J. Phys. Conf. Ser.* **2024**, *2909*, 012001. [CrossRef]
34. Gąska, D.; Haniszewski, T. Modelling studies on the use of aluminium alloys in lightweight load-carrying crane structures. *Transp. Probl.* **2016**, *11*, 13–20. [CrossRef]
35. Ntaskagianni, V. Aluminium in Modular Structures for Offshore Lifts. *Key Eng. Mater.* **2016**, *710*, 402–405. [CrossRef]
36. Plangger, J.; Schabhüttl, P.; Vuherer, T.; Enzinger, N. CMT additive manufacturing of a high strength steel alloy for application in crane construction. *Metals* **2019**, *9*, 650. [CrossRef]
37. Meissner, M.; Knecht, W.; Uszball, S.; Bartsch, H.; Feldmann, M.; Kuhlmann, U.; Knobloch, M. Structural behaviour of HSS hollow section K-joints–Experimental investigations and advanced numerical modelling using damage mechanics. *Steel Constr.* **2025**, *18*, 164–179. [CrossRef]
38. Petrović, A.; Momčilović, N.; Sedmak, A.; Đorđević, B.; Radu, D.; Milošević-Mitić, V.; Bogojević, A. Reliability-based approach for structural integrity assessment of a bucket wheel excavator. *Theor. Appl. Fract. Mech.* **2025**, *136*, 104849. [CrossRef]
39. Ashby, M.F. *Materials Selection in Mechanical Design*, 3rd ed.; Butterworth-Heinemann: Oxford, UK, 2005.
40. Tomasi, I.; Grandi, S.; Donzella, G.; Solazzi, L. Implementation of Composite Materials for Lightweighting of Industrial Vehicle Chassis. *J. Compos. Sci.* **2025**, *9*, 611. [CrossRef]
41. Toray Composite Materials America Inc. M50J High Modulus Carbon Fiber. Available online: https://cdn.thomasnet.com/ccp/30164375/140079.pdf (accessed on 18 June 2026).
42. Balasubramanian, M. *Composite Materials and Processing*; CRC Press: Boca Raton, FL, USA, 2014; Volume 711.
43. Mates Italiana, Product Data Sheet: SX10. Available online: https://fileserver.mates.it/Prodotti/2_Matrici/TDS/Resine/Mates/SX10_DS.pdf (accessed on 18 June 2026).
44. *EN 10025-1:2019*; Hot Rolled Products of Structural Steels—Part 1: General Technical Delivery Conditions. European Committee for Standardization (CEN): Brussels, Belgium, 2019.
45. *EN 755-2:2025*; Aluminium and Aluminium Alloys—Extruded Rod/Bar, Tube and Profiles—Part 2: Mechanical Properties. European Committee for Standardization (CEN): Brussels, Belgium, 2025.
46. Saimex s.r.l. Pultruded Bars and Profiles. 2018. Available online: https://saimex-pultrusion.com/pultruded-profiles/ (accessed on 3 May 2026).
47. Gude, M.; Lenz, F.; Gruhl, A.; Witschel, B.; Ulbricht, A.; Hufenbach, W. Design and automated manufacturing of profiled composite driveshafts. *Sci. Eng. Compos. Mater.* **2015**, *22*, 187–197. [CrossRef]
48. Arrabiyeh, P.A.; May, D.; Eckrich, M.; Dlugaj, A.M. An overview on current manufacturing technologies: Processing continuous rovings impregnated with thermoset resin. *Polym. Compos.* **2021**, *42*, 5630–5655. [CrossRef]
49. Solazzi, L. Feasibility of the tower crane jib made of composite material. In *IOP Conference Series: Materials Science and Engineering*; IOP Publishing: Bristol, UK, 2024; Volume 1306.
50. Solazzi, L.; Danzi, N. Jib crane lightweighting through composite material and prestressing technique. *Compos. Struct.* **2024**, *343*, 118283. [CrossRef]
51. Simiu, E.; Yeo, D. *Wind Effects on Structures: Modern Structural Design for Wind*; John Wiley & Sons: Hoboken, NJ, USA, 2019.
52. Holmes, J.D. *Wind Loading of Structures*; CRC Press: Boca Raton, FL, USA, 2018.
53. Konchakova, N.; Mueller, R.; Barth, F.-J. Modelling of damage evolution in adhesive metal-composite structures for various joint designs. *Mech. Control* **2011**, *30*, 213–220.
54. TEC s.r.l. Giunti, Apparecchi D'appoggio, Sistemi Antivibranti ed Antisismici per il Settore Civile, Industriale e Stradale. 2013. Available online: https://lancellottirestauro.com/wp-content/uploads/2013/07/tec-catalogo.pdf (accessed on 3 May 2026).
55. Ministero delle Infrastrutture e dei Trasporti. Aggiornamento delle «Norme Tecniche per le Costruzioni». Decreto Ministeriale 17 Gennaio 2018. Gazzetta Ufficiale n. 42 del 20 Febbraio 2018, Supplemento n. 8. Available online: https://www.gazzettaufficiale.it (accessed on 31 August 2026).
56. European Committee for Standardization (CEN). *Eurocodes: European Standards EN 1990–EN 1999 for Structural Design*; CEN: Brussels, Belgium, 2002.
57. Tran, Q.H.; Huh, J.; Nguyen, V.B.; Kang, C.; Ahn, J.-H.; Park, I.-J. Sensitivity Analysis for Ship-to-Shore Container Crane Design. *Appl. Sci.* **2018**, *8*, 1667. [CrossRef]
58. Ye, F.; Deng, H.; Fang, C.; Fu, X.; Li, Z. Damping Coefficient Calculation Method for Shore-Side Container Cranes under the Seismic Conditions. *Mech. Ind.* **2023**, *24*, 11. [CrossRef]
59. Li, Z.; Xu, C.; Wu, S. Calculating the Rayleigh damping coefficient under seismic dynamic simulation of a quayside container crane. *Aust. J. Mech. Eng.* **2022**, *20*, 44–53. [CrossRef]
60. Cimellaro, G.P.; Marasco, S. *Introduction to Dynamics of Structures and Earthquake Engineering*; Springer: Cham, Switzerland, 2018; Volume 45.
61. Feau, C.; Politopoulos, I.; Kamaris, G.S.; Mathey, C.; Chaudat, T.; Nahas, G. Experimental and numerical investigation of the earthquake response of crane bridges. *Eng. Struct.* **2015**, *84*, 89–101. [CrossRef]

62. Zheng, P.; Zhang, Q. Container cranes seismic load calculation criteria based on structural dynamics. In *2011 International Conference on Electric Information and Control Engineering*; IEEE: Piscataway, NJ, USA, 2011.
63. Belleri, A.; Labò, S.; Marini, A.; Riva, P. The influence of overhead cranes in the seismic performance of industrial buildings. *Front. Built Environ.* **2017**, *3*, 64. [CrossRef]
64. Solazzi, L.; Zrnic, N. Design of a high capacity derrick crane considering the effects induced by the application and the release of the load. *J. Appl. Eng. Sci.* **2017**, *15*, 15–24. [CrossRef]
65. Géradin, M.; Rixen, D.J. *Mechanical Vibrations: Theory and Application to Structural Dynamics*; John Wiley & Sons: Hoboken, NJ, USA, 2015.
66. Girard, A.; Roy, N. *Structural Dynamics in Industry*; John Wiley & Sons: Hoboken, NJ, USA, 2010; Volume 7.
67. Hu, S.C.; Zou, N.B.; Ouyang, S.; Zhang, W.Y. Simulation Analysis about Dynamic Characteristics of Crane's Jib System Based on the Lifting Loads. *Adv. Mater. Res.* **2014**, *910*, 304–307. [CrossRef]
68. Tomasi, I.; Solazzi, L. Dynamic Analysis of an Offshore Knuckle-Boom Crane Under Different Load Applications Laws. *Appl. Sci.* **2025**, *15*, 8100. [CrossRef]
69. Solazzi, L.; Zrnić, N. Mechanical behavior of ship to shore container crane subjected to different stochastic wind actions. In *Journal of Physics: Conference Series*; IOP Publishing: Bristol, UK, 2024; Volume 2647.

Disclaimer/Publisher's Note: The statements, opinions and data contained in all publications are solely those of the individual author(s) and contributor(s) and not of MDPI and/or the editor(s). MDPI and/or the editor(s) disclaim responsibility for any injury to people or property resulting from any ideas, methods, instructions or products referred to in the content.